Journal of Tribology, Volume 145, Issue 9, September 2023, Article number 091109
DOI:10.1115/1.4062720

Vibration analysis approach to model incremental wear and associated sound in multi-contact sliding friction mechanisms

Kanza Basit[1]
National University of Sciences and Technology (NUST)
Sector H-12, Islamabad, Pakistan
kanza.basit@pnec.nust.edu.pk

Hamza Shams
National University of Sciences and Technology (NUST)
Sector H-12, Islamabad, Pakistan
hamza.shams@pnec.nust.edu.pk

Cranfield University
Cranfield, United Kingdom

Muhammad Ali Khan
Cranfield University
Cranfield, United Kingdom
muhammad.a.khan@cranfield.ac.uk

Asif Mansoor
National University of Sciences and Technology (NUST)
Sector H-12, Islamabad, Pakistan
drasifmansure@pnec.nust.edu.pk

ABSTRACT

This paper proposes a simplistic approach towards estimating incremental wear in a multi-contact scenario using a vibrational analysis approach and in turn goes a step forward to model its associated sound. Predicted wear depth and frictional sound are compared to the experimental values obtained using a standardized pin-on-disc tribometer setup affixed with a free-field microphone to capture airborne noise. The results show good conformity between the proposed analytical model values and the standardized

[1] Corresponding Author: Kanza Basit
kanza.basit@pnec.nust.edu.pk

experiments, hence ensuing that within certain limitations, the proposed model and the intended approach can effectively be used as a good estimator of wear and its sound in a multi-contact scenario.

Introduction

It has been well-established that evaluation of associated parameters in a sliding contact such as surface roughness, wear rate, wear noise, etc., can be used for efficient condition-based monitoring (CBM) in machines and systems [1–6]. The tribological conditions present during sliding is of great benefit for predictive maintenance (PM) in machines and tools and can therefore be used to assess component life [7–11]. There are various methods for diagnosing machine wear parameters to improve its life, with one of them being acoustic and wear analysis either online or offline [12–15]. The online in-situ wear analysis of a machine component is considered to be the better and more realistic method to predict wear.

Various predictive models [16–20] for estimation of wear and its associated properties have been developed in the past and validated for their efficiency through experimental analysis. [21–25] In particular, wear due to friction between sliding contacts has attracted greater interest of researchers due to its effectiveness in gear motion, brake application, and other similar interactions between mechanical components. [26–28] Correspondingly, the associated noise generated when two or more material components interact with each other is also considered to be a valuable parameter in predicting the failure of machines. [29,30] These models take into the consideration the equipment conditions and wear prognosis evaluated by surface roughness estimation, incremental analysis, Archard wear, frequency analysis, and vibration-based diagnostics. [31,32]

Conventionally, these vibration-based models predict wear progress at an advanced stage of contact. However, an initial sliding between materials also tends to produce an elastic penetration causing a frictional noise to generate which is directly linked to the interaction between the materials involved. [33–35] Frictional noise can thus also be used as a reliable indicator of the predicted damage that a component may undergo. Variation in frictional noise and wear have been found to be directly related in various vibration-based wear estimation models. [36–38]

Vibration models associated with the prediction of wear in terms of sound analysis are typically based on simulation of brake squeal noise and instability analysis of a machine using a pin-on-disc setup. [39,40] Although, most of the studies are based on one pin contact with the disc but in order to replicate a machine environment, more than one point of contact is also considered within a single machine component. [41,42]

Double pin model to predict the instabilities in a running machine have been previously approximated using acoustics and vibrations confirming the presence and origination of 'squeal' noise in disc-brakes. [43–45] This has been further improved with the addition of damping parameters. [46] These studies have provided an understanding of complex vibration analysis with generalized results but have limitations in defining unstable regions during sliding of brake-pad. A simplified simulation considering dynamic interactions between brake pads and the calipers has also been presented using two actuators and frictional guides, where the proposed mathematical model has been further validated by laboratory experiments. Although these results also show conformity

between the model and the experiments, its scope is widely reserved to modeling of contact force. [47]

To overcome these limitations, our research group has previously used sound parameters (such as RMS of microphone voltage and cumulative amplitudes of dominant frequencies) to evaluate wear in mechanical elements with multiple contact points under load. Although our model shows a good correlation of wear and sound parameters for a variety of conditions, it was widely limited to empirical analysis. [2,48]

It is therefore widely understood that limitations in wear and sound prediction when multiple elements interact persist. However, at the same time vibration-based models have proven to be an integral predictive technique for both wear and sound. Taking this into consideration, we present a simplistic vibration-based model using spring-mass system to study wear depth caused by the lateral movement of pin and its associated frictional noise on interaction with a rotating disc. An analytical model has been presented by considering a two-pin-on-disc setup assembled as a spring-mass system which makes uses variable loads and pin materials to attribute for varying sliding contact conditions. Incremental wear depth is predicted over the pre-defined sliding distance for both the pins and consequently, frictional noise is also computed using vibration signal and corresponding sound analysis. The model is then validated by using a conventional pin-on-disc setup equipped with a custom-designed two-pin holder and a free-field microphone, in order to allow two pins to slide over a single disc at the same time and capture the corresponding frictional noise. Evaluation of results yields good conformity

with the approximations with minimal error which shows that the model can be effectively used to estimate tool life degradation.

Analytical Model

It is important to evaluate the expected efficient life of a machine component in order to increase or maintain productivity. An analytical model helps in estimation of threshold (critical) parameters to avoid abrupt failure in machines. The proposed model is developed by considering two pins sliding on a single disc. The pin-on-disc mechanism is considered to be a simplistic undamped spring-mass system, where the disc has torsional stiffness due to rotation while the pins have a lateral stiffness since they are affixed from the top.

Figure 1 shows the proposed spring-mass system where two pins with stiffness, k_1 and k_2 respectively, slide over a disc. The disc has a torsional stiffness denoted by k_{t1} and k_{t2} with respect Pin 1 and Pin 2 respectively.

To specify the model constraints, the following assumptions are set at the starting stage.

1. The disc is considered to be a thin circular plate (t<6 mm) therefore deflection due to shear maybe neglected.
2. The contact is considered to be a point contact at indentation therefore Hertz contact theory is applicable.
3. The pin initially comes in contact with the disc and then slides over it for a small period of time (elastic deformation) finally wearing out the disc (wearing out phase).
4. The pin is considered to move downward only, i.e., no lateral movement or rotation.

5. The disc is supposed to rotate and consequently wear occurs as pin(s) penetrate inside the thickness of the disc.
6. Wear on pin is negligible

This results in the system's behavior being classified as undamped with free vibration and defined by Equation 1.[49]

$$x(t) = x_0 cos\omega_n t + \frac{\dot{x_0}}{\omega_n} sin\omega_n t \quad (1)$$

Where, $x(t)$ is the pin's displacement with time t, ω_n is the natural frequency of the system and x_0 is the pin's initial starting position and $\dot{x_0}$ it's first derivative. The detailed solution for the evaluation of these parameters is provided in **S1**.

Wearing out Phase

When wear occurs, pins slide over a solid thin disc of mild steel on a number of contact points. Wear depth defined as L_1 and L_2 for the two pins can be approximated at each point where the summation of wear depth at all points in accordance with Hertz contact model [50] and the classic wear theory proposed by Jia et al. [51] which is a modified form of Archard wear model [52] for macro-level analysis then leads to the evaluation of cumulative wear depth for a pre-defined sliding distance. At each point, it is assumed that the contact is that of a sphere-on-flat surface type as the pins have a spherical contact end, and therefore, Hertz contact model for similar configuration can be adopted.

The stiffness equation 2 below for the rotating disc as specified in **S1** assumes that G, shear modulus of the disc and D, diameter of the disc remains constant, therefore

equation 2 can be re-written as equation 3 which shows that the contact depth varies with time.

$$K_{tn} = GJ/L_n \quad (2)$$

Where K_{tn}, is the time-dependent stiffness, J is the polar moment of inertia and L_n is the contact depth which is equal to the ball's diameter, acting as a pin.

$$K_{tn} = (\pi G D^4)/32h_{i+1} \quad (3)$$

Where h_{i+1} is the incremental wear depth corresponding to L_n.

The modified Archard wear model, equation 4 can now be used to quantify wear on the disc. The original model proposed by Archard is the most common wear prediction tool based on the theory of asperities contact, whereas the modified version takes into consideration macro-level parameters as shown below.

$$V = \frac{skF}{H} \quad (4)$$

Where V is the wear volume, s is the sliding distance, k is a dimensionless wear constant, F is the normal force and H is the hardness factor.

For a Hertzian contact [53], the contact radius, a, with an effective radius R is defined by equation 5.

$$a = \sqrt[3]{\frac{3FR}{4E}} \quad (5)$$

Where F is the normal force and E is the effective Young's Modulus at the contact defined by equation 6.

$$\frac{1}{E} = \frac{1}{2}\left(\frac{1-\vartheta_p^2}{E_p} + \frac{1-\vartheta_d^2}{E_d}\right) \quad (6)$$

Here E_p and E_d are the Young's Modulus of pin and disc respectively, while ϑ_p and ϑ_d are the Poisson's ratio of the pin and disc respectively. The effective radius R is also dependent on the pin (R_p) and disc (R_d) radius as shown in equation 7.

$$\frac{1}{R} = \frac{1}{R_p} + \frac{1}{R_d} \quad (7)$$

To evaluate wear depth as a function of sliding force and the initial elastic deformation we now make use of the Global Increment Wear Model (GIWM) [54]. The GIWM for predicting wear on disc is based on the assumption that the contact area evolves in shape of an ellipse and therefore, the contact length (minor axis of the contact ellipse), $2a_H$ decreases with progressive sliding while the wear track width (major axis of the contact ellipse), $2a$ increases over sliding as shown by the dotted ellipse in Figure *2*. The initial elastic deformation can then be evaluated using equation 8.

$$h_o^e = F/2Ea_o \quad (8)$$

Where, h_o^e is the initial elastic deformation, F is the normal force, E is the effective Young's Modulus and $2a_o$ is the initial track width.

Initially, the contact radius, a, is calculated using Hertz contact theory as per equation 5. At this point the contact area is considered to be circular therefore, the major axis is equal to the minor axis. However, as wear progresses the contact area increases thereby decreasing the contact pressure over the sliding distance.

Through iterative computations, wear and deformation can then be evaluated for each revolution of the pins on the disc till the maximum sliding distance is reached as shown by the GIWM flowchart in **S1**. The first step to this process is the calculation of incremental wear using integral of the linear wear from GIWM, as shown in equation 9.

$$h_{i+1}^{w} = h_{i}^{w} + 2k_{D}p_{i}a_{Hi} \quad (9)$$

Where, h_{i+1}^{w} incremental wear depth at point '$i+1$' with respect to sliding distance, h_{i}^{w} is the wear depth at point 'i' with respect to sliding distance. k_D is the stiffness of the disc and p_i is the average contact pressure based on the applied normal load which can be evaluated using equation 10.

$$p_{i} = \frac{F}{\pi a_{i+1}a_{Hi}} \quad (10)$$

The elastic deformation normal to the contact can then be evaluated using Oliver and Pharr relationship [55] used in the GIWM as given by equation 11.

$$h_{i+1}^{e} = \frac{F}{2E\sqrt{a_{i+1}a_{Hi}}} \quad (11)$$

For elliptical contact, the initial contact length a_{Hi} then takes the form of equation 12.

$$a_{Hi} = 2\sqrt{\frac{FR}{\pi a_{i+1}\pi E}} \quad (12)$$

Where π is a correction factor.

The total wear depth then becomes a function of h_i^e, initial elastic deformation and h_{i+1}^{w}, incremental wear depth as shown in equation 13.

$$h_{i+1} = h_{i}^{e} + h_{i+1}^{w} \quad (13)$$

By substituting h_{i+1}, the total wear depth in equation 3, the time dependent stiffness of the disc (torsional stiffness) simplifies to equation 14.

$$K_{tn} = \frac{\pi G D^4}{32(h_i^e + h_{i+1}^w)} \quad (14)$$

The natural frequency of the system which is function of disc and pin stiffness as discussed in **S1** can now be evaluated by assigning an estimated value for mass. The outputs of these equations are then substituted back in equation 1 to evaluate pin displacement as a function of time. The initial displacement x_0 can be evaluated using equation 15 [54,55].

$$x_0 = \frac{F}{2Ea} \quad (15)$$

The first derivative of $x_0, \dot{x}_0$, the angular velocity of the disc is assumed to be a constant due to fixed revolutions per minute and for our use, we assume a value of 250 rpm.

The equation 1 now simplifies to equation 16:

$$x(t) = \frac{F}{2Ea} cos\omega_n t + \frac{250}{\omega_n} sin\omega_n t \quad (16)$$

Frictional Noise

To calculate frictional noise, we make use of the acoustic power formulation [56] as given in equation 17.

$$P = \rho_0 c S \sigma V^2 \quad (17)$$

Where ρ_0= air density, c = speed of sound in air, S = cross sectional surface area, σ = radiation efficiency (can be taken as 1), and V = vibrational velocity. The vibrational

velocity is calculated by taking a time derivative of equation 16, which leads to the formation of equation 18 below.

$$V(t) = -\frac{F\omega_n}{2Ea} sin\omega_n t + 250 cos\omega_n t \quad (18)$$

The sound power level is given by equation 19:

$$L_w = 10\ log_{10}\left(\frac{P}{P_r}\right) \quad (19)$$

Where, P_r is the reference power equal to 10^{-12} W. The sound pressure level is then given by equation 20.

$$L_{p1} = L_w + 10\ log_{10}\left(\frac{Q}{4\pi r^2}\right) \quad (20)$$

Where, Q is the directivity factor equal to either 1 (full sphere propagation), 2 (half sphere propagation), 4 (quarter sphere propagation) or 8 (eighth sphere propagation). The sound pressure then simplifies to equation 21.

$$P = P_0 * 10^{\frac{1}{20}L_{p1}} \quad (21)$$

Where, P_0 is the reference pressure equal to 20x10^{-6} Pa.

To validate that our assumptions hold, an experimental scheme was developed to compare the analytical and experimental results of total wear depth, (equation 13) and the sound pressure (equation 21).

Experimental Scheme

To investigate wear depth and the sound pressure experimentally, a standardized pin-on-disc tribometer, TRB^3 by Anton Paar is utilized with a specialized free-field microphone,

GRAS 40PP (sensitivity 47.46 mV/Pa @ 250 Hz). The microphone is mounted at a fixed distance of 50 mm from the pin/disc assembly.

The tribometer has a cantilever arm which allows direct measurement of the combined wear depth (penetration depth) and associated friction parameters. For the purpose of multi-contact, we use a custom designed pin-holder capable of holding 2 balls in contact with the disc as shown in Figure 3. The design is inspired from the single ball holder provided with the Tribometer. There are two hollow cylinders for holding two balls at the same time, with threads on the top so that it can be fixed by a steel rod. The disc rotates with a constant velocity of 250 rpm while the balls slide over it, causing wear and frictional noise.

The pin holder is calibrated prior to the setup to show that the results obtained from the one-ball holder configuration are an approximate average of the wear results obtained from the two-ball holder [2].

The microphone records the frictional noise in the form of sound pressure. The microphone is connected to NI SignalExpress using NI 9234 DAQ card affixed on a NI 9174 chassis for in-situ recording at synchronized fixed time intervals. The complete experimental setup is shown in Figure 4.

A zoomed version of the experimental and analytical setups is shown in Figure 5 for comparison. Table 1 lists the physical specifications of the pin-and-disc materials used in our investigations.

The specifications of the experiments performed for validation of the proposed analytical model based on spring-mass system are described in Table 2. A range of loads and materials were varied to study the efficiency of the model over a wider spectrum of varying parameters. Some of the proposed models in the past have performed well at low loads while there have been discrepancies and large error associated when load on each disc-pin pair is increased. Therefore, it is imperative to validate the model at high loads as well as low loads. However, due to the operational limitations in our experimental setup, we were not able to increase the load beyond 30 N without triggering the equipment safety limit. Disc materials used were Mild Steel (MS) and Aluminum (Al) as both are widely available in academic as well as industrial setting for contact analysis and are extensively used for machine elements manufacturing.

MS disc experiments were performed at a fixed 250 rpm speed while for Al the speed was increased to 400 rpm as Al is a slightly brittle material and it wears out at a higher rate as compared to MS, thus, reaching the threshold coefficient of friction (COF) values incorporated by the Tribometer software causing the experiment to stop prematurely as a safety precaution.

Wear tracks on the sample were then analyzed using Taylor Hobson CCI Optical 3D Profiler with white light filter using 20x magnification lens to obtain track profiles (width and depth) and average them over the track length to generate a general wear profile. Tests were repeated 3-4 times to confirm repeatability of results.

Comparison of Results

The proposed analytical model is validated with the experimental results. Figure 6 shows the comparison total wear depths (penetration depths), while Figure 7 shows the variation in sound pressure between analytical and experimental models based on the parameters specified in Table 2.

It can be seen from Figure 6 and Figure 7 that experimental and analytical results are in good correlation with each other over the specified range of loads. Measurements were recorded for three incremental loads on each pin. It is pertinent to mention that a conventional increase in wear depth is observed with addition of load. Similarly, for sound results, sound pressure increases with an increase in loads on each pin. When a 10 N load is applied, wear rate is measured to be under 25 microns, however, once load is increased to 20 N, a sudden increase in wear depth is observed. At 20 N, wear depth goes up to about 50 microns which is almost double the measurements at 10 N. However, when the load increases to 30 N, the wear depth increases slightly more than 20 N measurements to about 60 microns. Experimental wear graphs can be seen to be good in conformance with the analytical wear. For additional validation of the experimental wear, the samples are also observed under a 3D optical profiler as shown in Figure 8 where the wear depth results obtained are in close conformance to those obtained from the tribometer.

Towards the end of the measurement cycle, it can be observed that individual instantaneous wear depth decreases. The maximum wear therefore occurs during the first 2 minutes of the experiment for mild steel as per the hardness of the material. As the pins continue to slide over the mild steel disc, a very small amount of wear generates at

each point, however, incremental wear is always increasing. Thus, a clear discrepancy is observed at the end of high load cycles because a very small amount of point wear is added to the incremental wear towards the end of the cycle.

Sound pressure was recorded using a microphone and the data was extracted from SignalExpress project file and imported to MATLAB for further analysis. The sound measurements recorded were considered to be averaged sound pressure with respect to both the pins. Anomalous high pressure values were filtered out and the graphs were replotted for comparison with the analytical sound pressure. A clear increase in sound pressure is observed with load. At the same time, it showed conformance with the analytical/projected sound. Sound pressure measurements at 10 N, almost doubles when the load is increased to 20 N, similar to what appears in the wear results. The error is recorded under 20% for all loads, with the maximum error at 10 N readings as shown in Figure 9.

A significant increase in wear depth is observed for aluminum discs in Figure 10. It is because, Al is more prone to wear and degradation as compared to harder material like MS or any other steel component. Furthermore, the pins used are made of Stainless Steel, which has a much higher hardness than aluminum alloys. For Al discs, it was observed that maximum wear occurs in the first 20 seconds of the experiment due to its brittleness, contrary to 2 minutes in the case of mild steel discs. Additionally, the incremental wear depth increases only slightly with addition of loads. Consequently, the sound pressure also increases with load. Error associated with Al and SS pin-disc combinations for load conditions is illustrated in Figure 11.

Further Validation

The model was initially formulated for MS-SS316-SS316 contact condition and replicated over Al-SS316-SS316 as shown in Figure 6, Figure 7 and Figure 10 previously. To validate the model further, we replaced one of the pin (ball) with SS52100 to make the two combinations of MS-SS316-SS52100 and Al-SS316-SS52100 respectively. SS52100 has higher mechanical strength as opposed to the other pin made of SS316.

As can be seen from Figure 12 and Figure 13, the analytical results are still good representative of the experimental wear and sound because of the use of effective values instead of individual material constants in our base model. However, at the same time it can also be observed that the percentage error has now increased which means that the unequal wear generated by the contact of different material combinations is now being captured by the tribometer and the average wear progresses at a faster rate.

Conclusion

A solution towards evaluating incremental wear in a multi-contact sliding friction mechanism has been presented in the form of a vibrational analysis model. The model's constants are derived from existing wear models for single pin-on-disc combinations whereas the model variables are being driven by the system's assumed or actual parameters. Figure 14 presents a quick summary of the model presented in this paper.

The proposed work is clear evidence that by using a more simplified vibrational analysis approach, it is possible to model incremental wear and its associated sound in a multi-contact sliding friction mechanism. Furthermore, through experimentation, it is also shown that that the use of expensive contact sensors for machine life diagnosis can be

replaced by using inexpensive predictive maintenance tools which use air-borne noise as a parameter for precision diagnosis in a continuously operating machine.

In this article an incremental model for computing wear on disc and its corresponding sound at contact in a multiple pin-on-disc setup has been presented. The foundation of the model is based on spring-mass systems associated with each pin and disc combination. Tribological tests to validate the proposed analytical model show conformity in terms of analytical and empirical results for both wear and frictional sound. Wear and sound increase drastically in low hardness material, like Al, over the pre-set period of experiment due to their vulnerability to wear out quickly as compared to relatively hard material, like Mild Steel. In addition, a combination of different pins yields close results but with increased error percentage.

Therefore, following are some key contributions that have been identified in our work and can be used for further studies on multi-contact sliding friction setups.

1. In a first, this paper presents a possibility for evaluating incremental wear and its associated sound during multi-contact sliding friction system (two pins-on-disc system) by modeling it as a simple undamped spring-mass system.
2. The proposed vibrational analysis model takes into consideration the GIWM, Archard's principle and Hertzian contact models which are commonly used in a single-pin (ball) systems to evaluate equation constants. For variable quantities, the model effectively makes use of actual/ assumed system parameters to provide solution for incremental wear depth and its associated sound pressure as shown in Figure 14.

3. The analytical results are then validated experimentally using a custom designed pin-on-disc setup on a standardized tribometer affixed with a microphone for recording airborne noise. Following are the summarized observations from the experiments:
    a. Wear depth and sound pressure for all experiments are in close correlation to the analytical/predicted wear and sound.
    b. For all experiments, incremental wear depth increases with the addition of load and consequently, sound pressure also increases.
    c. An average wear depth of maximum 60 microns (for 30 N load) was recorded for MS disc and SS316 pins configuration
    d. However, with a change in one of the pins materials to SS52100, it was observed that the maximum wear depth is below 60 microns (for 30 N load) due to one of the pins having higher hardness property as compared to the other. Similar results were obtained for sound pressure.
    e. For an Aluminum disc, maximum wear depth is achieved much quicker than MS due to material properties
    f. However, for different hardness pins sliding on an aluminum disc, the maximum wear depth is recorded only slightly less than that of two same material pins configuration.
    g. Similarly, the sound pressure recorded is lesser for two different material pins configuration.

h. A second validation of the experimental wear depth is carried out using a 3D optical profiler which effectively shows that the wear depth obtained directly from the tribometer penetration depth sensor and that from the 3D optical profile are in good congruence with each other.

4. Using the vibration model, it is possible to evaluate wear on higher load values (in the range of N) as compared to the existing wear models such as GIWM which only considers small loads in the range of mN.

The vibration analysis route for evaluating incremental wear and its associated sound for a multi-contact sliding friction system has been reported for the first time which overcomes the limitation presented by earlier models such as those based on asperity contacts [57]. The work therefore addresses an important knowledge gap for investigation of wear parameters in more realistic multi-contact system and subsequent work is required for optimizing the model further with the aim to reduce the overall system error which is directly linked to the specific materials in contact and their surface properties.

FUNDING

This work is jointly supported by Cranfield University, UK and National University of Sciences and Technology (NUST), Pakistan with one co-author supported by the Commonwealth Scholarship Commission, grant number PKCN-2019-405.

REFERENCES

[1] Borghesani, P., Smith, W. A., Zhang, X., Feng, P., Antoni, J., and Peng, Z., 2018, "A New Statistical Model for Acoustic Emission Signals Generated from Sliding Contact in Machine Elements," Tribol Int, **127**, pp. 412–419.

[2] Basit, K., Shams, H., Khan, M. A., and Mansoor, A., 2020, "Empirical Modelling of Frictional Noise and Two-Point Contact Using Ball-On-Disc Tribometer," SSRN Electronic Journal.

[3] Khan, M. A., Hussnain, R. B., Basit, K., Safdar, M., and Raza, M., 2013, "Effect of Lubricant on Wear Debris Color Diagnosis," Journal of Mechanical Engineering and Technology (JMET) , **5**(2), pp. 89–99.

[4] Wang, L., Sheng, X., and Luo, J., 2022, "A Peridynamic Frictional Contact Model for Contact Fatigue Crack Initiation and Propagation," Eng Fract Mech, **264**, p. 108338.

[5] Wang, L., Duan, J., He, M., Liu, Y., and Bao, Y., 2022, "Study on Antifriction Mechanism of Surface Textured Elliptical Bearings," J Tribol, pp. 1–20.

[6] Yin, N., Xing, Z., He, K., and Zhang, Z., 2023, "Tribo-Informatics Approaches in Tribology Research: A Review," Friction, **11**(1), pp. 1–22.

[7] Raadnui, S., 2019, "Spur Gear Wear Analysis as Applied for Tribological Based Predictive Maintenance Diagnostics," Wear, **426–427**, pp. 1748–1760.

[8] Vianna, W. O. L., and Yoneyama, T., 2018, "Predictive Maintenance Optimization for Aircraft Redundant Systems Subjected to Multiple Wear Profiles," IEEE Syst J, **12**(2), pp. 1170–1181.

[9] Shams, H., Basit, K., Khan, M. A., Mansoor, A., and Saleem, S., 2021, "Scalable Wear Resistant 3D Printed Slippery Liquid Infused Porous Surfaces (SLIPS)," Addit Manuf, **48**, p. 102379.

[10] Shams, H., Basit, K., Khan, M. A., and Mansoor, A., 2020, "Wear Behavior of 3D Printed PLA Surfaces for Superhydrophobic Interaction," SSRN Electronic Journal.

[11] Shahid, M. A., Khan, T. M., Lontin, K., Basit, K., and Khan, M., 2020, "Multiple Point Contact Wear Prediction and Source Identification Scheme Using a Single Channel Blended Airborne Acoustic Signature," IFAC-PapersOnLine, **53**(3), pp. 283–288.

[12] Geng, Z., Puhan, D., and Reddyhoff, T., 2019, "Using Acoustic Emission to Characterize Friction and Wear in Dry Sliding Steel Contacts," Tribol Int, **134**, pp. 394–407.

[13] Shanbhag, V. v., Rolfe, B. F., Arunachalam, N., and Pereira, M. P., 2018, "Investigating Galling Wear Behaviour in Sheet Metal Stamping Using Acoustic Emissions," Wear, **414–415**, pp. 31–42.

[14] Lychagin, D. V., Filippov, A. V., Kolubaev, E. A., Novitskaia, O. S., Chumlyakov, Y. I., and Kolubaev, A. V., 2018, "Dry Sliding of Hadfield Steel Single Crystal Oriented to Deformation by Slip and Twinning: Deformation, Wear, and Acoustic Emission Characterization," Tribol Int, **119**, pp. 1–18.

[15] Wang, J., Huo, L., Liu, C., Peng, Y., and Song, G., 2018, "Feasibility Study of Real-Time Monitoring of Pin Connection Wear Using Acoustic Emission," Applied Sciences, **8**(10), p. 1775.

[16] Yan, W., O'Dowd, N. P., and Busso, E. P., 2002, "Numerical Study of Sliding Wear Caused by a Loaded Pin on a Rotating Disc," J Mech Phys Solids, **50**(3), pp. 449–470.
[17] Rigney, D. A., 1988, "Sliding Wear of Metals," *Annual Review of Materials Science*, pp. 141–163.
[18] Jahangiri, M., Hashempour, M., Razavizadeh, H., and Rezaie, H. R., 2012, "Application and Conceptual Explanation of an Energy-Based Approach for the Modelling and Prediction of Sliding Wear," Wear, **274–275**, pp. 168–174.
[19] Noraphaiphipaksa, N., Kanchanomai, C., and Mutoh, Y., 2013, "Numerical and Experimental Investigations on Fretting Fatigue: Relative Slip, Crack Path, and Fatigue Life," Eng Fract Mech, **112–113**, pp. 58–71.
[20] Karupannasamy, D. K., Kailas, S. V., Shankar, S., and Sasikumar, K. S. K., 2022, "A Predictive Model for Galling Phenomenon and Its Applicability for Deep Drawing Processes," J Tribol, **144**(1).
[21] Dhope, K., and Tallur, S., 2018, "Analytical Model for Monitoring of AFM Tip Wear through Resonance Frequency Measurements," *2018 4th IEEE International Conference on Emerging Electronics (ICEE)*, IEEE, pp. 1–4.
[22] Teymuri Sindi, C., 2019, "Development of an Acoustic Emission Model for Adhesive Wear," Mater Eval, **77**(4), pp. 529–534.
[23] Stavropoulos, P., Papacharalampopoulos, A., and Souflas, T., 2020, "Indirect Online Tool Wear Monitoring and Model-Based Identification of Process-Related Signal," Advances in Mechanical Engineering, **12**(5), p. 168781402091920.
[24] Zhou, Y., Peng, M., Zuo, X., and Xu, J., 2022, "Correlation Between Friction Coefficient and Friction Vibration in Running-In Process Based on Cross Recurrence Plots," J Tribol, **144**(1).
[25] Hasan, M. S., Kordijazi, A., Rohatgi, P. K., and Nosonovsky, M., 2022, "Triboinformatics Approach for Friction and Wear Prediction of Al-Graphite Composites Using Machine Learning Methods," J Tribol, **144**(1).
[26] Guilbault, R., and Lalonde, S., 2019, "A Stochastic Prediction of Roughness Evolution in Dynamic Contact Modelling Applied to Gear Mild Wear and Contact Fatigue," Tribol Int, **140**, p. 105854.
[27] Feng, K., Ni, Q., and Zheng, J., 2022, "Vibration-Based System Degradation Monitoring under Gear Wear Progression," Coatings, **12**(7), p. 892.
[28] Ma, W., Li, X., Wang, Q., and Jiang, X., 2022, "Theoretical Analysis of the Effects of Grain Size and Orientation on Rail Damage," Eng Fract Mech, **259**, p. 108148.
[29] le Bot, A., 2017, "Noise of Sliding Rough Contact," J Phys Conf Ser, **797**, p. 012006.
[30] Xu, J. Y., Mo, J. L., Huang, B., Wang, X. C., Zhang, X., and Zhou, Z. R., 2018, "Reducing Friction-Induced Vibration and Noise by Clearing Wear Debris from Contact Surface by Blowing Air and Adding Magnetic Field," Wear, **408–409**, pp. 238–247.
[31] Josue da Silva, P., and Alvares, A. J., 2020, "Investigation of Tool Wear in Single Point Incremental Sheet Forming," Proc Inst Mech Eng B J Eng Manuf, **234**(1–2), pp. 170–188.

[32] Yang, Y. Y., 2013, “Solutions of Dissimilar Material Contact Problems,” Eng Fract Mech, **100**, pp. 92–107.
[33] Zhang, H., Wang, W., Zhang, S., and Zhao, Z., 2017, “Modeling of Elastic Finite-Length Space Rolling-Sliding Contact Problem,” Tribol Int, **113**, pp. 224–237.
[34] Wang, X. C., Mo, J. L., Ouyang, H., Wang, D. W., Chen, G. X., Zhu, M. H., and Zhou, Z. R., 2016, “Squeal Noise of Friction Material With Groove-Textured Surface: An Experimental and Numerical Analysis,” J Tribol, **138**(2).
[35] Zhang, Z., Yin, N., Chen, S., and Liu, C., 2021, “Tribo-Informatics: Concept, Architecture, and Case Study,” Friction, **9**(3), pp. 642–655.
[36] Xiang, Z. Y., Mo, J. L., Ouyang, H., Massi, F., Tang, B., and Zhou, Z. R., 2020, “Contact Behaviour and Vibrational Response of a High-Speed Train Brake Friction Block,” Tribol Int, **152**, p. 106540.
[37] Wang, H., Liu, Z., Zou, L., and Yang, J., 2017, “Influence of Both Friction and Wear on the Vibration of Marine Water Lubricated Rubber Bearing,” Wear, **376–377**, pp. 920–930.
[38] Yonemura, S., Zhou, L., and Talke, F. E., 2003, “An Investigation of Slider Vibrations in Near Contact Recording Using a Digital Laser Doppler Vibrometer,” J Tribol, **125**(3), pp. 571–575.
[39] Lazzari, A., Tonazzi, D., and Massi, F., 2019, “Squeal Propensity Characterization of Brake Lining Materials through Friction Noise Measurements,” Mech Syst Signal Process, **128**, pp. 216–228.
[40] Denimal, E., Nacivet, S., Nechak, L., and Sinou, J.-J., 2017, “On the Influence of Multiple Contact Conditions on Brake Squeal,” Procedia Eng, **199**, pp. 3260–3265.
[41] Sanchez-Marin, F., Roda-Casanova, V., and Porras-Vazquez, A., 2018, “A New Analytical Model to Predict the Transversal Deflection under Load of Stepped Shafts,” Int J Mech Sci, **146–147**, pp. 91–104.
[42] Khafidh, M., Setiyana, B., Jamari, J., Masen, M. A., and Schipper, D. J., 2018, “Understanding the Occurrence of a Wavy Wear Track on Elastomeric Materials,” Wear, **412–413**, pp. 23–29.
[43] Earles, S. W. E., and Badi, M. N. M., 1984, “Oscillatory Instabilities Generated in a Double-Pin and Disc Undamped System: A Mechanism of Disc-Cbrake Squeal,” Proc Inst Mech Eng C J Mech Eng Sci, **198**(1), pp. 43–50.
[44] Earles, S. W. E., and Badi, M. N. M., 1978, “On the Interaction of a Two-Pin-Disc System with Reference to the Generation of Disc-Brake Squeal.”
[45] Zerbst, U., Lundén, R., Edel, K.-O., and Smith, R. A., 2009, “Introduction to the Damage Tolerance Behaviour of Railway Rails – a Review,” Eng Fract Mech, **76**(17), pp. 2563–2601.
[46] Earles, S. W. E., and Chambers, P. W., 1987, “Disc Brake Squeal Noise Generation: Predicting Its Dependency on System Parameters Including Damping,” International Journal of Vehicle Design, **8**, pp. 538–552.
[47] Sen, O. T., Dreyer, J. T., and Singh, R., 2013, “Low Frequency Dynamics of a Translating Friction Element in the Presence of Frictional Guides, as Motivated by a Brake Vibration Problem,” J Sound Vib, **332**(22), pp. 5766–5788.

[48] Khan, M., Basit, K., Khan, S., Khan, K., and Starr, A., 2017, "Experimental Assessment of Multiple Contact Wear Using Airborne Noise under Dry and Lubricated Conditions," Proceedings of the Institution of Mechanical Engineers, Part J: Journal of Engineering Tribology, **231**(12), pp. 1503–1516.
[49] Rao, S. S., 2019, "Derivation of Equations," *Vibration of Continuous Systems*, John Wiley & Sons, Inc., Hoboken, NJ, USA, pp. 69–85.
[50] Machado, M., Moreira, P., Flores, P., and Lankarani, H. M., 2012, "Compliant Contact Force Models in Multibody Dynamics: Evolution of the Hertz Contact Theory," Mech Mach Theory, **53**, pp. 99–121.
[51] Jia, K., and Fischer, T. E., 1997, "Sliding Wear of Conventional and Nanostructured Cemented Carbides," Wear, **203–204**, pp. 310–318.
[52] Archard, J. F., 1953, "Contact and Rubbing of Flat Surfaces," J Appl Phys, **24**(8), pp. 981–988.
[53] Johnson, K. L., 1982, "One Hundred Years of Hertz Contact," Proceedings of the Institution of Mechanical Engineers, **196**(1), pp. 363–378.
[54] Hegadekatte, V., Huber, N., and Kraft, O., 2006, "Modeling and Simulation of Wear in a Pin on Disc Tribometer," *Part A: Tribomaterials; Lubricants and Additives; Elastohydrodynamic Lubrication; Hydrodynamic Lubrication and Fluid Film Bearings; Rolling Element Bearings; Engine Tribology; Machine Components Tribology; Contact Mechanics*, ASME, pp. 567–575.
[55] Oliver, W. C., and Pharr, G. M., 1992, "An Improved Technique for Determining Hardness and Elastic Modulus Using Load and Displacement Sensing Indentation Experiments," J Mater Res, **7**(6), pp. 1564–1583.
[56] Harrison, M., 2004, "Interior Noise: Assessment and Control," *Vehicle Refinement*, Elsevier, pp. 145–233.
[57] Lontin, K., and Khan, M. A., 2021, "Wear and Airborne Noise Interdependency at Asperitical Level: Analytical Modelling and Experimental Validation," Materials, **14**(23), p. 7308.

Figure Captions List

Figure 1 - Analytical model of spring-mass system

Figure 2: Evolution of wear track in the form of an ellipse. [54]

Figure 3: (A) Multi-contact custom pin (ball) holder and (B) shows the eccentric mounting of the pin holder on the disc to obtain visibly different wear tracks at 2 contact points [2].

Figure 4: The experimental pin-on-disc setup for recording wear depth and sound pressure.

Figure 5: Comparison between the experimental (left) and analytical (right) setups.

Figure 6: Comparison of analytical and experimental total wear depth results plotted against time based on the experimental scheme defined in Table 2.

Figure 7: Comparison of analytical and experimental sound pressure results plotted against time based on the experimental scheme defined in Table 2.

Figure 8: Validation of total wear depth parameter using the Taylor Hobson CCI Optical 3D profiler (Laser Interferometer) to cross-reference values with experimental values obtained from the tribometer with MS-SS316-SS316 where (A) 10 N, (B) 20 N and (C) 30 N.

Figure 9: Error percentage between analytical and empirical results in (A) Total wear depth, and (B) Sound pressure for MS-SS316-SS316.

Figure 10: Comparison of analytical and empirical results of Total Wear Depth (Left) and Sound Pressure (Right) obtained for Al-SS316-SS316 combination for (A) 10 N, (B) 20 N and (C) 30 N.

Figure 11: Error percentage between analytical and empirical results in (A) Total wear depth, and (B) Sound pressure for Al-SS316-SS316.

Figure 12: Comparison of analytical and empirical results of Total Wear Depth (Left) and Sound Pressure (Right) obtained for MS-SS316-SS52100 combination for (A) 10 N, (B) 20 N and (C) 30 N.

Figure 13: Comparison of analytical and empirical results of Total Wear Depth (Left) and Sound Pressure (Right) obtained for Al-SS316-SS52100 combination for (A) 10 N, (B) 20 N and (C) 30 N.

Figure 14: Flowchart of Vibrational Analysis model for incremental wear and sound during multi-contact sliding in undamped condition

Table Caption List

Table 1: Standard pin and disc configurations used in the investigation.

Table 2: Experimental setup for validation of the analytical model

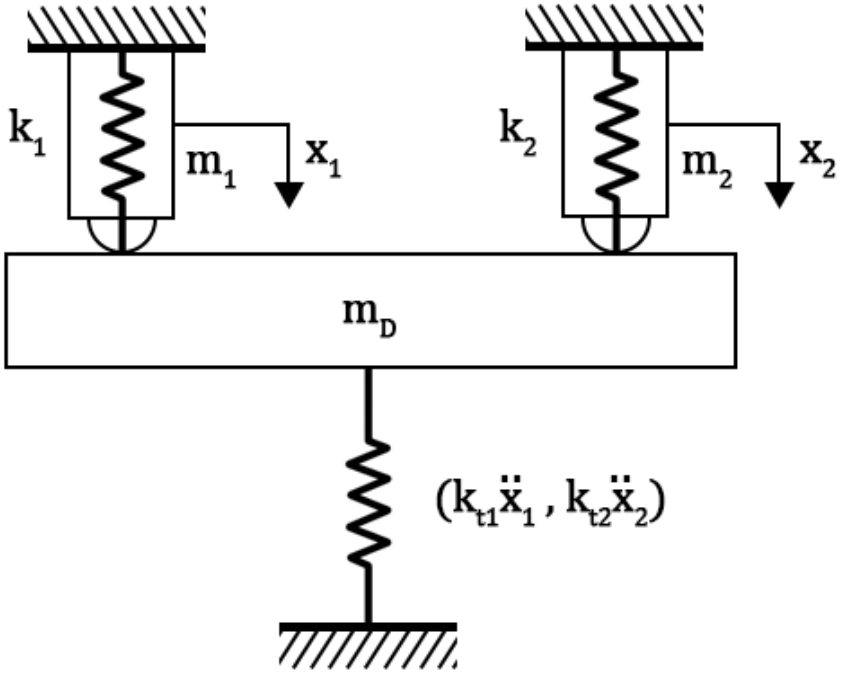

Figure 1 - Analytical model of spring-mass system

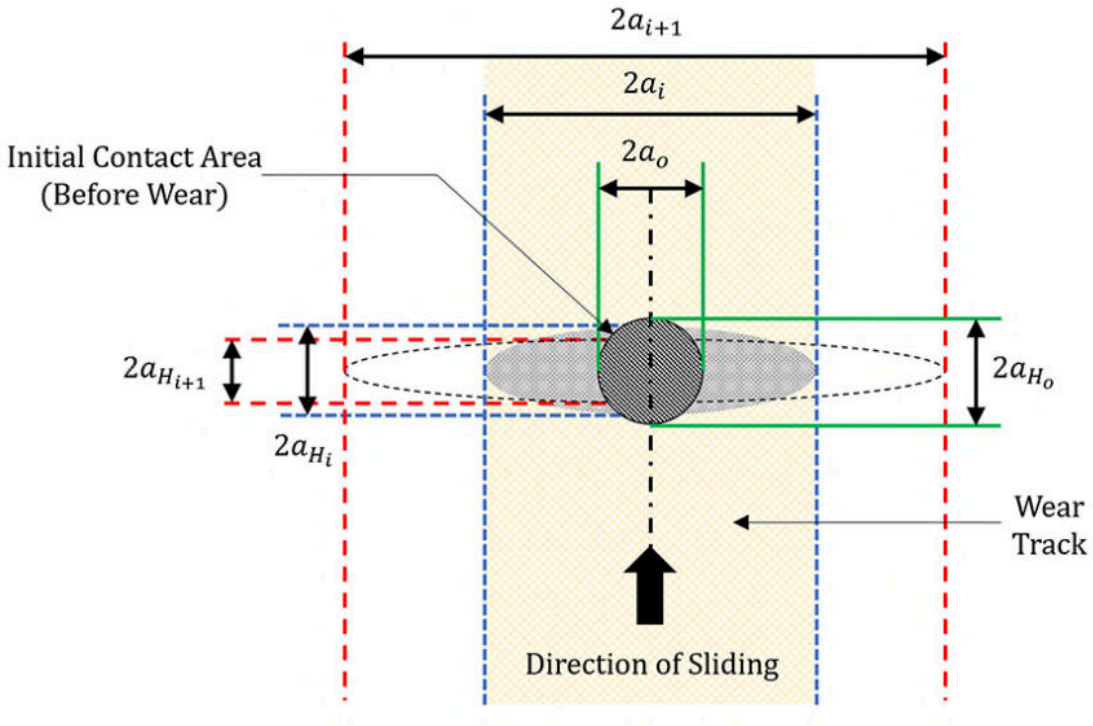

Figure 2: Evolution of wear track in the form of an ellipse. [54]

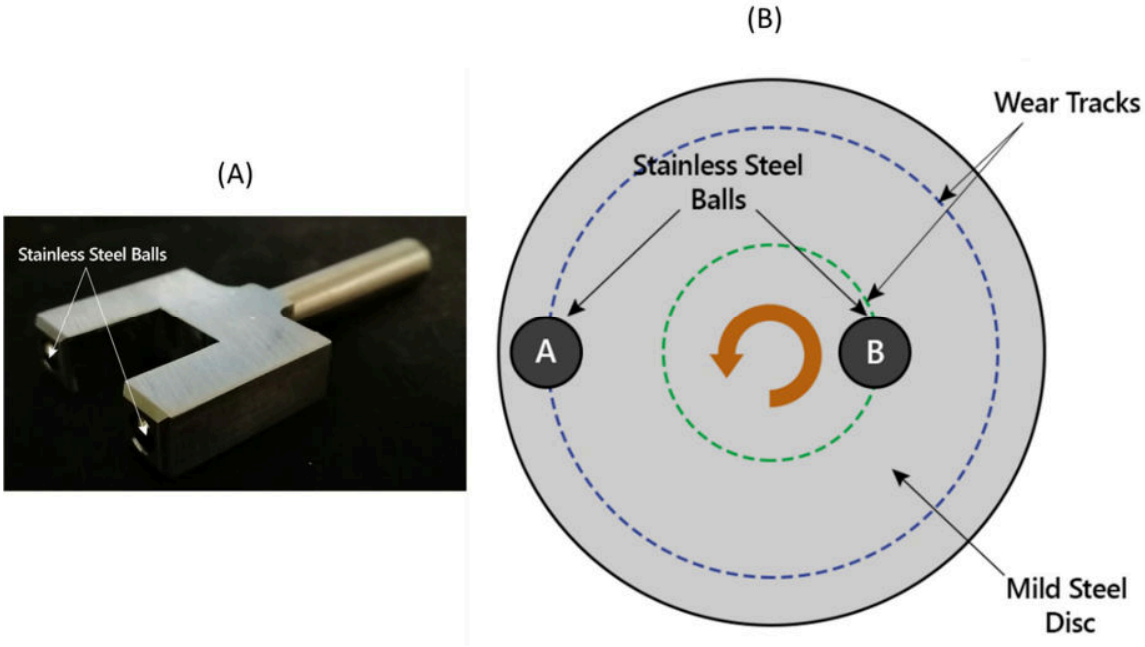

Figure 3: (A) Multi-contact custom pin (ball) holder and (B) shows the eccentric mounting of the pin holder on the disc to obtain visibly different wear tracks at 2 contact points [2].

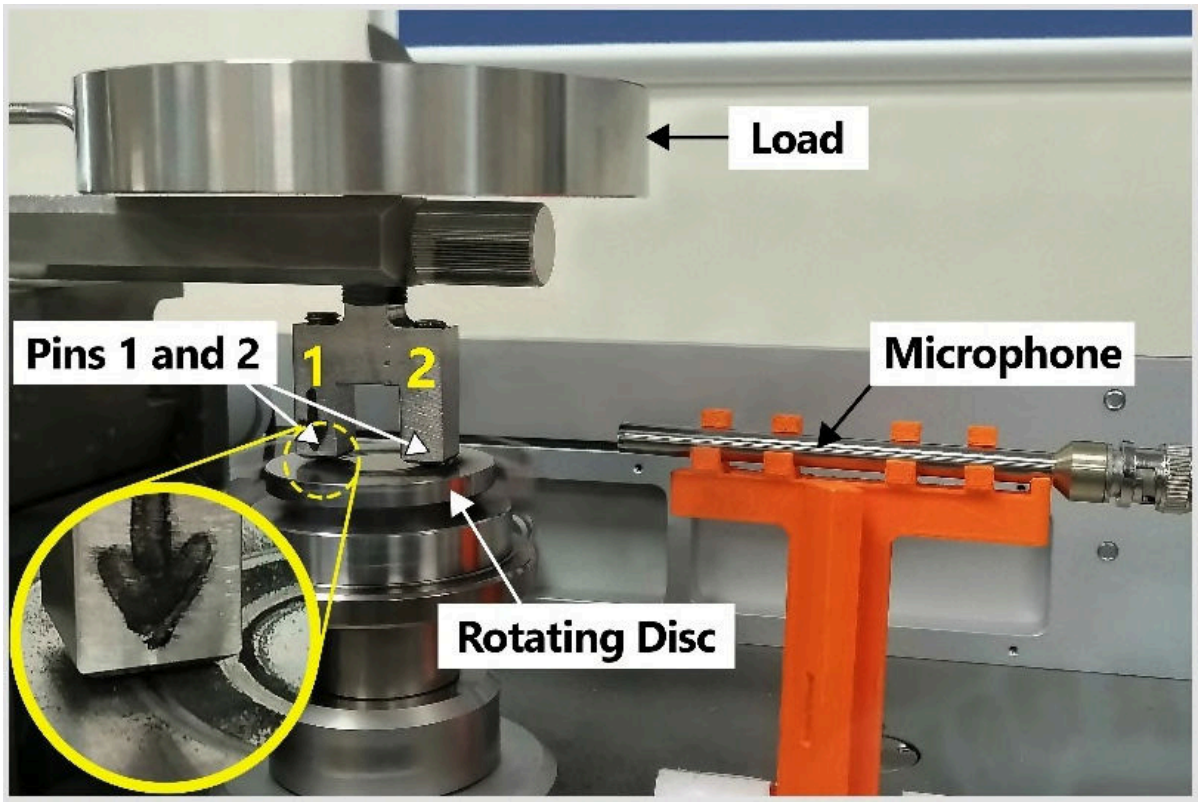

Figure 4: The experimental pin-on-disc setup for recording wear depth and sound pressure.

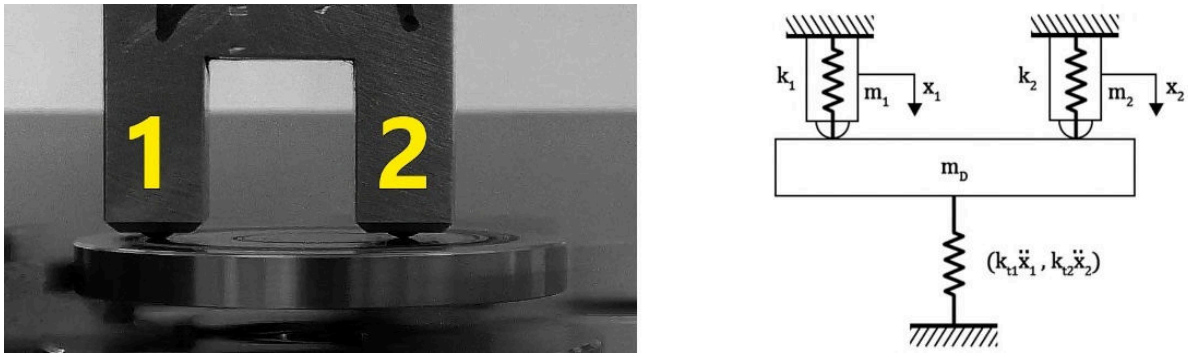

Figure 5: Comparison between the experimental (left) and analytical (right) setups.

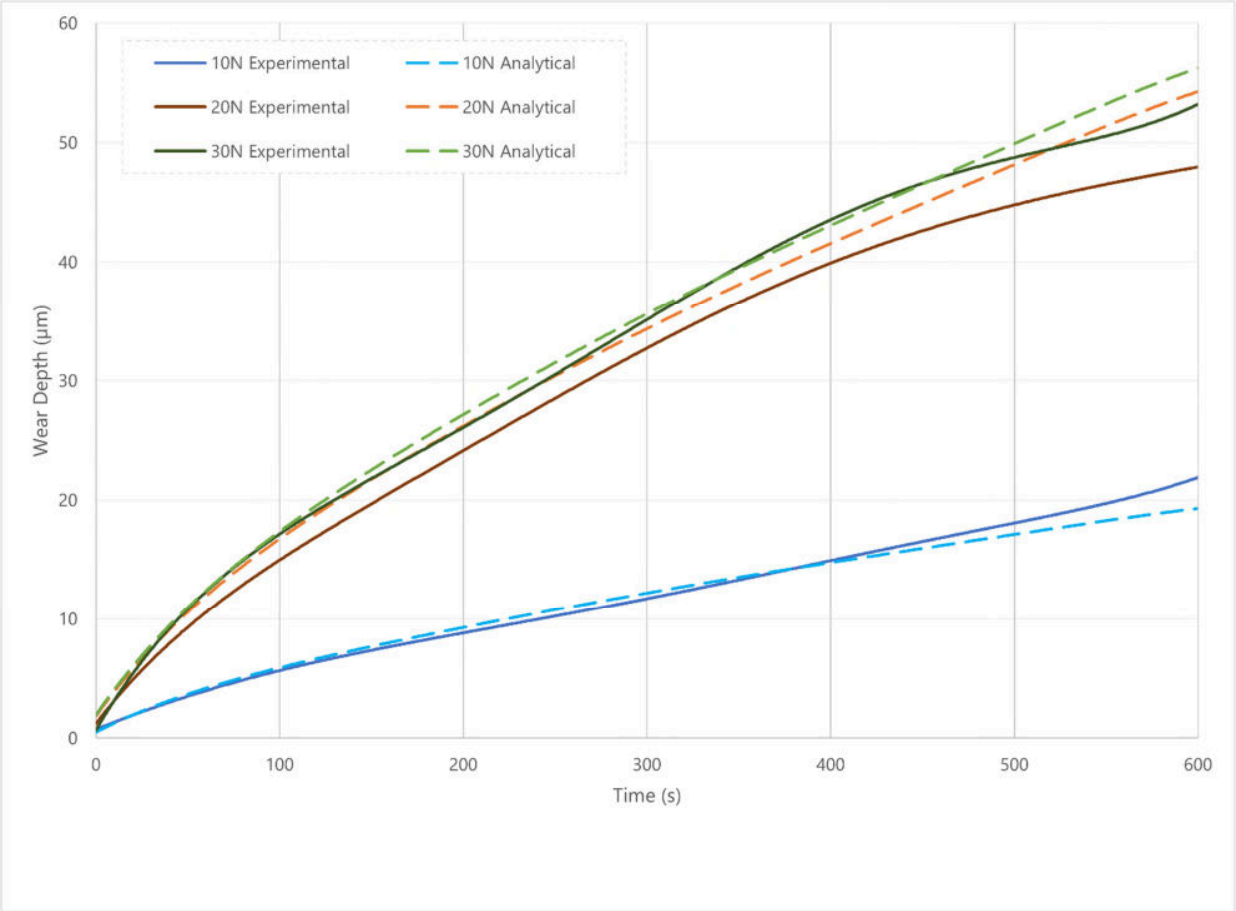

Figure 6: Comparison of analytical and experimental total wear depth results plotted against time based on the experimental scheme defined in Table 2.

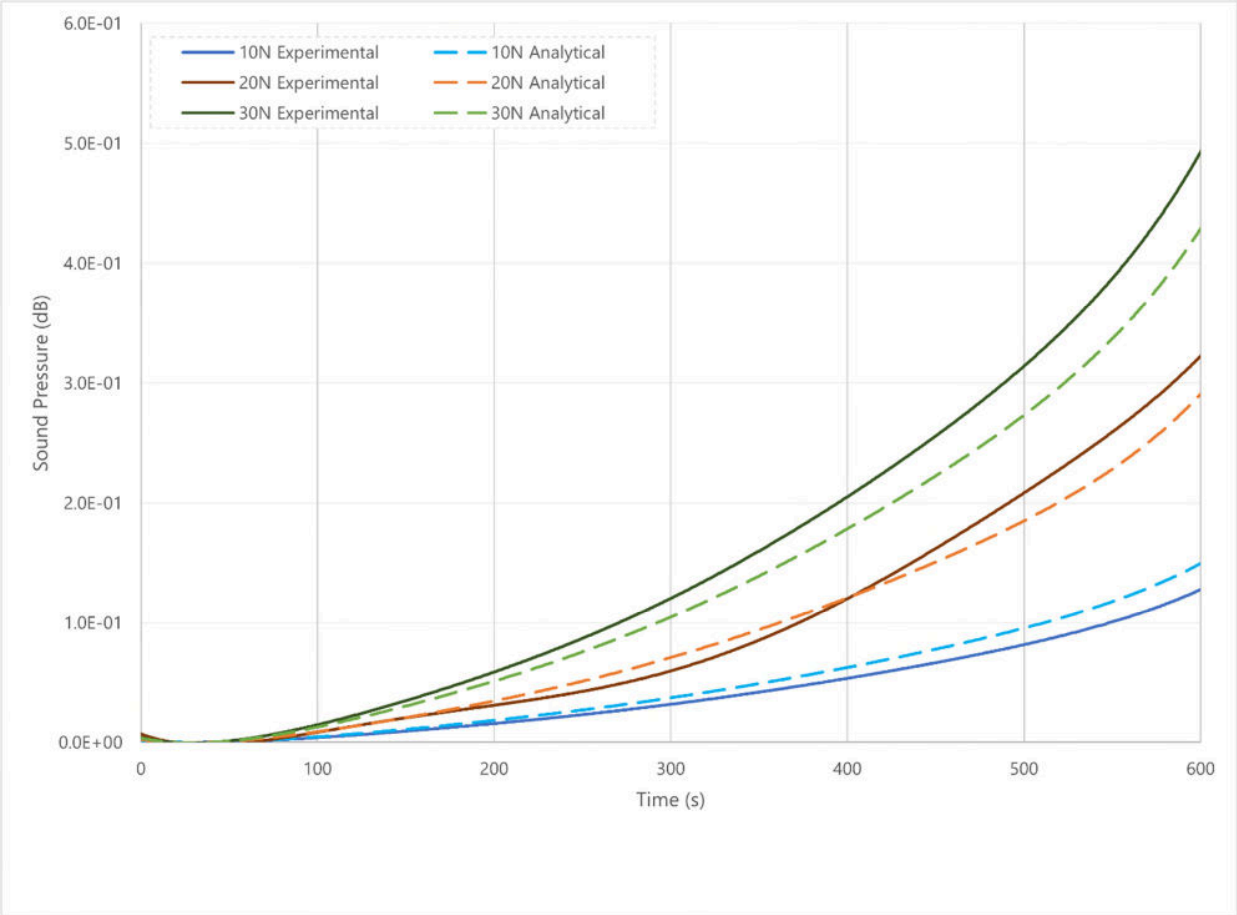

Figure 7: Comparison of analytical and experimental sound pressure results plotted against time based on the experimental scheme defined in Table 2.

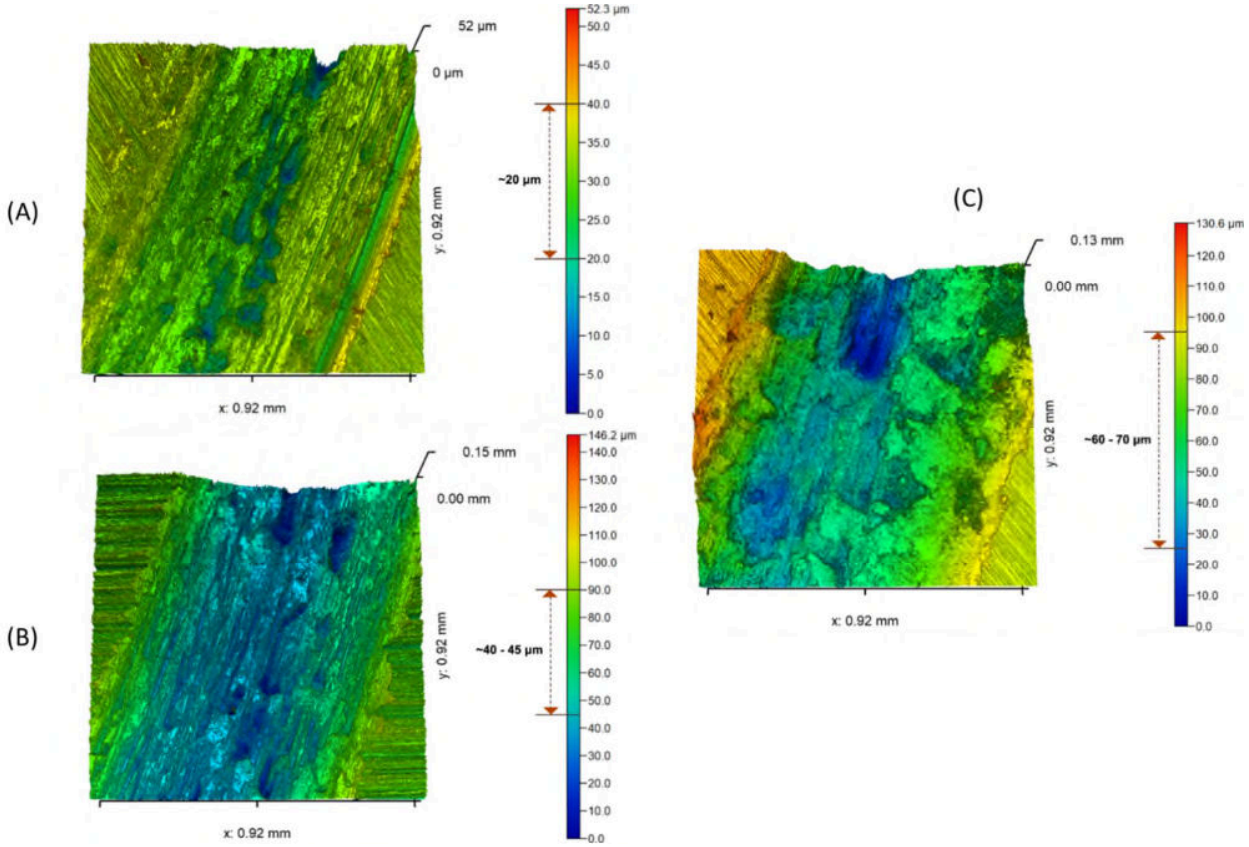

Figure 8: Validation of total wear depth parameter using the Taylor Hobson CCI Optical 3D profiler (Laser Interferometer) to cross-reference values with experimental values obtained from the tribometer with MS-SS316-SS316 where (A) 10 N, (B) 20 N and (C) 30 N.

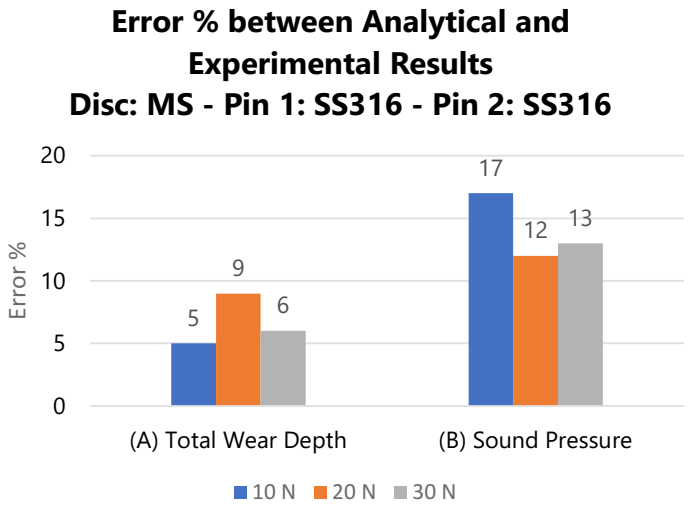

Figure 9: Error percentage between analytical and empirical results in (A) Total wear depth, and (B) Sound pressure for MS-SS316-SS316.

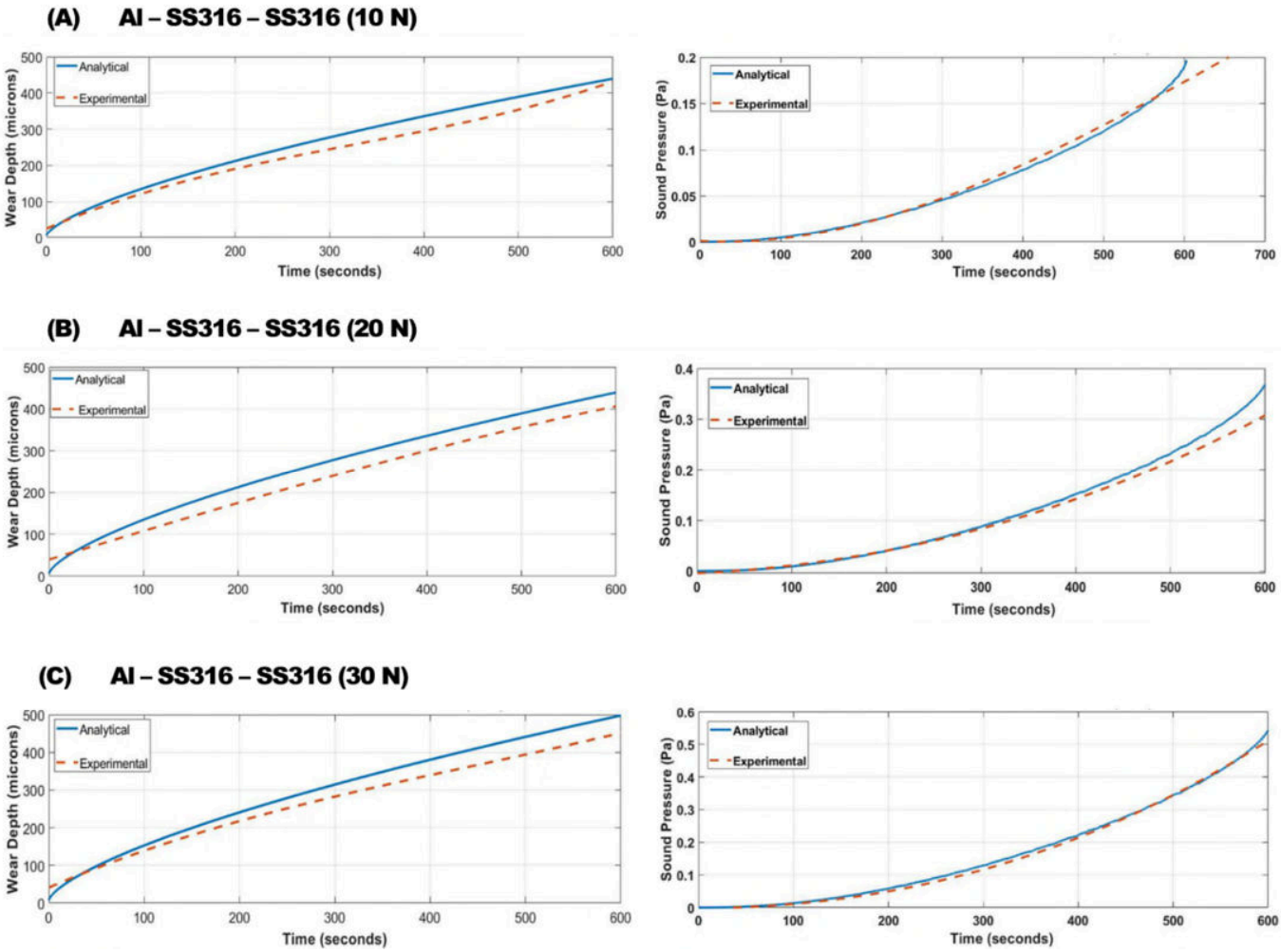

Figure 10: Comparison of analytical and empirical results of Total Wear Depth (Left) and Sound Pressure (Right) obtained for Al-SS316-SS316 combination for (A) 10 N, (B) 20 N and (C) 30 N.

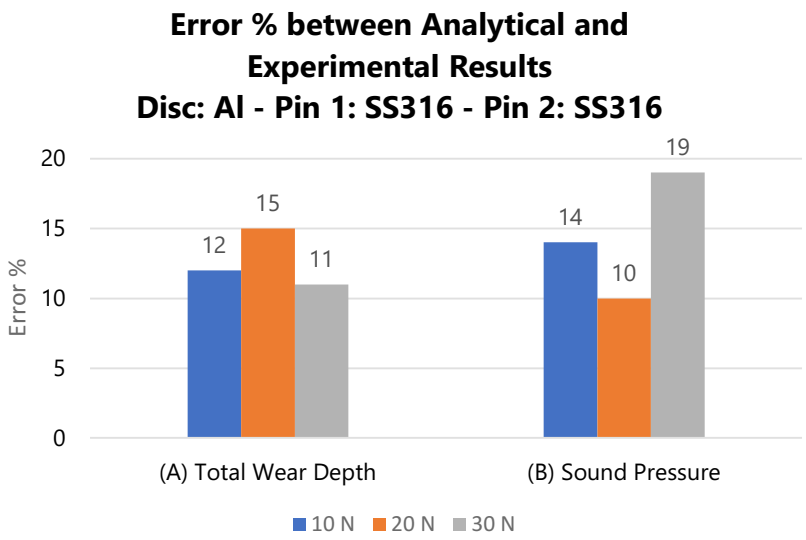

Figure 11: Error percentage between analytical and empirical results in (A) Total wear depth, and (B) Sound pressure for Al-SS316-SS316.

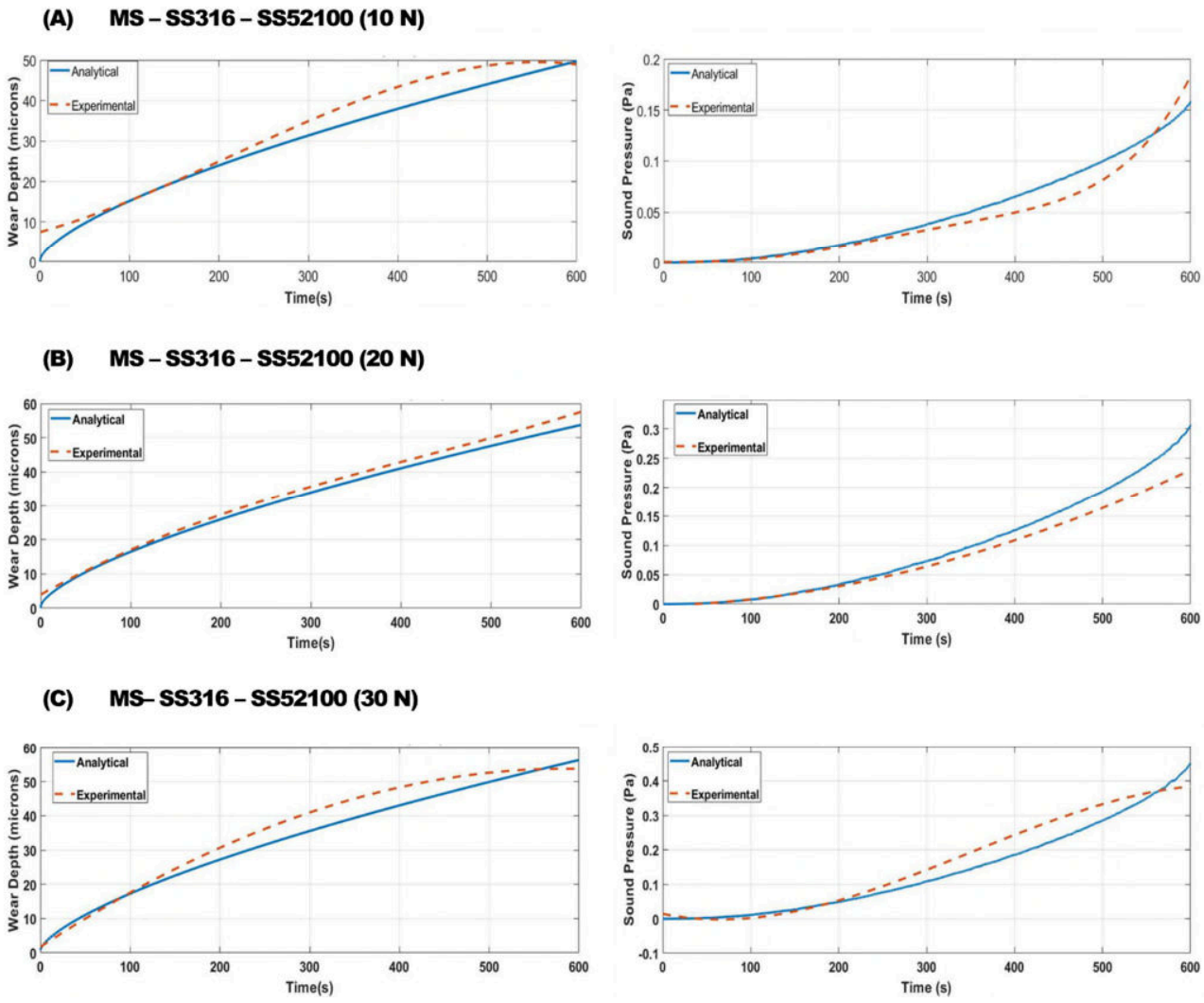

Figure 12: Comparison of analytical and empirical results of Total Wear Depth (Left) and Sound Pressure (Right) obtained for MS-SS316-SS52100 combination for (A) 10 N, (B) 20 N and (C) 30 N.

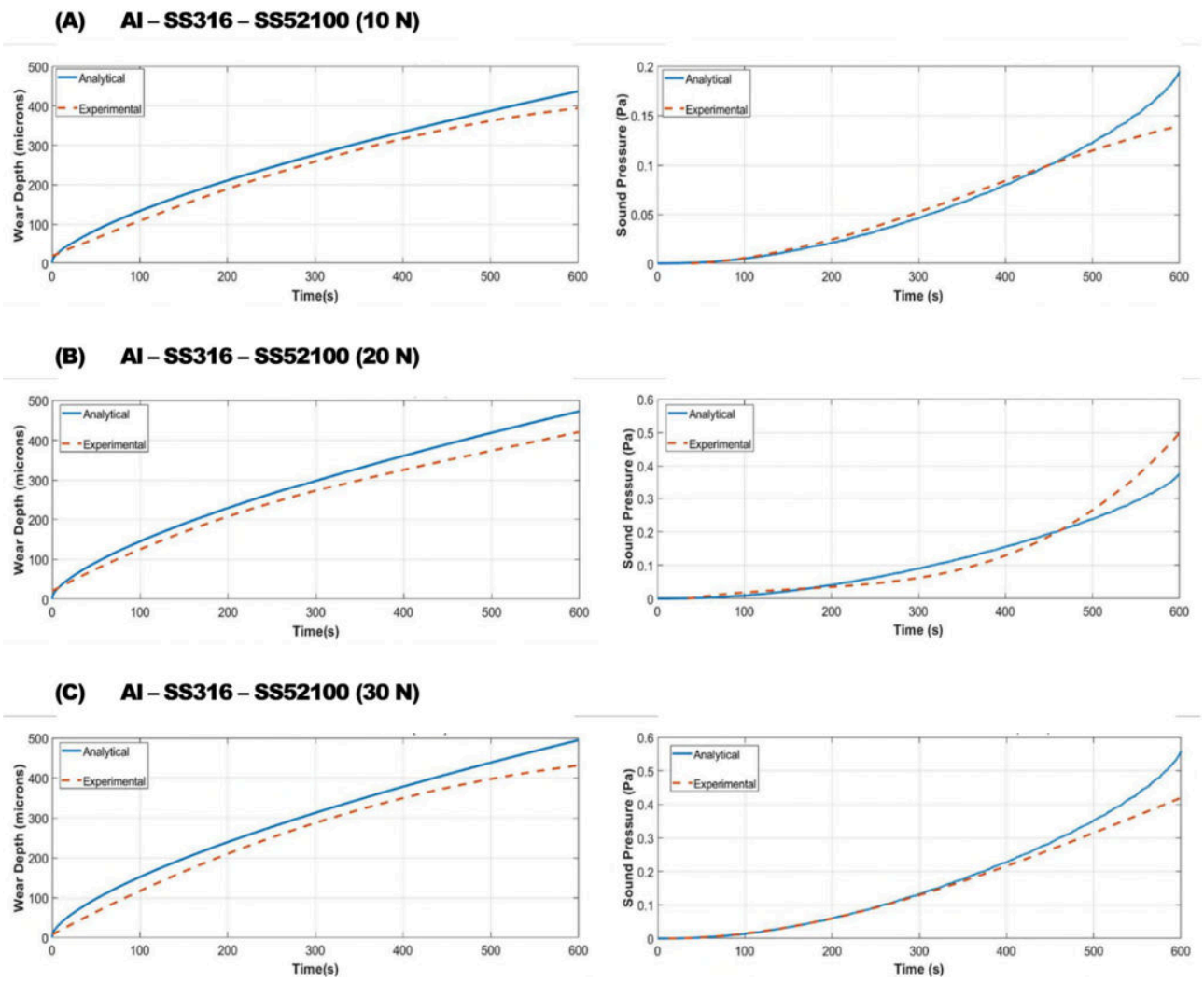

Figure 13: Comparison of analytical and empirical results of Total Wear Depth (Left) and Sound Pressure (Right) obtained for Al-SS316-SS52100 combination for (A) 10 N, (B) 20 N and (C) 30 N.

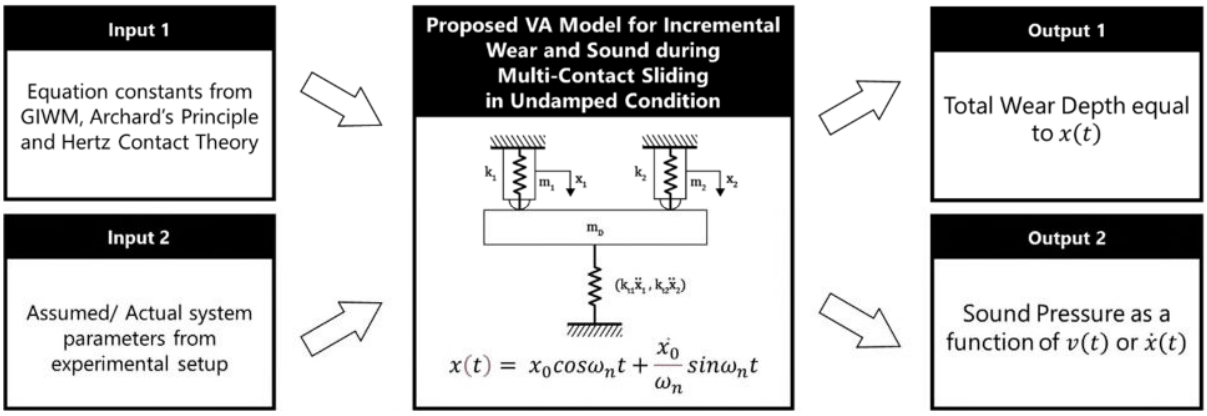

Figure 14: Flowchart of Vibrational Analysis model for incremental wear and sound during multi-contact sliding in undamped condition

Table 1: Standard pin and disc configurations used in the investigation.

Item	Material	Diameter (mm)	Speed (rpm)
Pin 1	Stainless Steel (SS 316/SS 52100)	6	0 (Fixed)
Pin 2	Stainless Steel (SS 316/SS 52100)	6	0 (Fixed)
Disc	Mild Steel (MS)	50	250

Table 2: Experimental setup for validation of the analytical model

Speed (rpm)	Pin Material	External Load (N)	Disc Material
250	Pin 1: SS 316 Pin 2: SS 316	10	MS
		20	
		30	
400		10	Al
		20	
		30	

2023-07-04

Vibration analysis approach to model incremental wear and associated sound in multi-contact sliding friction mechanisms

Basit, Kanza

American Society of Mechanical Engineers

Basit K, Shams H, Khan MA, Mansoor A. (2023) Vibration analysis approach to model incremental wear and associated sound in multi-contact sliding friction mechanisms. Journal of Tribology, Volume 145, Issue 9, September 2023, Article number, 091109

https://doi.org/10.1115/1.4062720